Top-down pathways to devices with few and single atoms placed to high precision

New Journal of Physics
The open-access journal for physics

Top-down pathways to devices with few and single atoms placed to high precision

Jessica A Van Donkelaar[1], Andrew D Greentree, Andrew D C Alves, Lenneke M Jong, Lloyd C L Hollenberg and David N Jamieson

Centre for Quantum Computer Technology, School of Physics, The University of Melbourne, Melbourne, Victoria 3010, Australia
E-mail: j.vandonkelaar@pgrad.unimelb.edu.au

New Journal of Physics **12** (2010) 065016 (19pp)
Received 4 December 2009
Published 28 June 2010
Online at http://www.njp.org/
doi:10.1088/1367-2630/12/6/065016

Abstract. Solid-state devices that employ few and single atoms are emerging as a consequence of technological advances in classical microelectronics and proposals for quantum computers based on spin or charge. The fabrication of devices in both these areas requires the development of techniques for deterministic doping of silicon where few or single dopant atoms must be placed to, typically, nanometre precision. Here we discuss a top-down approach, based on deterministic ion implantation, which can potentially be used to fabricate devices intended to explore the novel challenges of designing, building and measuring solid-state devices at the single atom limit. In particular, we address the potential of fabricating more complex devices that exploit quantum coherence. We propose a prototype triple-donor device that transports electron spin qubits via the coherent tunnelling by adiabatic passage (CTAP) protocol for a scalable quantum computer. We examine theoretically the statistics of dopant placement using ion implantation by employing an analytical treatment of CTAP transport properties under hydrogenic assumptions. We evaluate the probability of fabricating proof of concept devices subject to the limitations of ion implantation. We find that the results are promising with a yield of one in six for 14 keV phosphorus implanted into silicon with a target atom site spacing of 30 nm with even higher yields possible for lower-energy implants. This suggests that deterministic doping is an important tool to fabricate and test near-term practical quantum coherent devices.

[1] Author to whom any correspondence should be addressed.

Contents

1. Introduction

In a remarkable convergence of imperatives, the International Technology Roadmap for Semiconductors [1] and the rise of quantum computer technology [2] in the solid state both present significant challenges for the engineering of atoms in semiconductor devices. In the first case, scaling of MOSFETs to the 22 nm level and below will mean large statistical fluctuations in the number and location of dopants, leading to undesirable sharp increases in the statistical variability of the threshold voltage compared to previous generations. A means to control this variability must be developed. Also, the impact of quantum effects at these small scales needs to be assessed. In the second case, these quantum effects form the basis of the device function and again require the precise location of dopant atoms in nano-scale CMOS devices with a comparable precision.

A potential solution to these challenges is the emerging technique of deterministic doping. Several variations of this technique are being developed based on atomic-precision hydrogen-resist lithography [3], or counted ion implantation [4–6]. New proposals for the use of laser-cooled ions in the ion source of an ion implantation system could deliver arrays of single ions with nanometre spatial precision [7–9]. These techniques could be used to construct small-scale, solid-state quantum coherent devices to test the viability of, for example, charge-qubit operations [10] or quantum transport [11]. In the future, hydrogen-resist lithography [12] promises large-area atomic scale precision, necessary to build a large-scale scalable quantum computer [13, 14].

We propose here the near-term fabrication of prototype devices by ion implantation. Our technique makes use of a conventional ion implanter teamed with methods to count the number of ions implanted into controlled positions in a semiconductor device. By removing the statistical variations of blanket implantations, considerably improved device properties and inter-device variability are expected and observed [15].

Quantum devices require quantum transport so that information can be effectively handled. Here, we concentrate on the feasibility of quantum transport via the coherent tunnelling adiabatic passage (CTAP) protocol [11]. Specifically, we focus on strategies for constructing a three-donor device in phosphorus in silicon, which is intended to test the CTAP protocol. The CTAP protocol is reviewed in section 2, along with new analytical results that enable efficient determination of the required timescales in non-optimal geometries. These results lead to efficient criteria to determine the theoretical device yields used later. Progress towards a

scanned aperture system to perform the implants is described in section 3. In sections 4 and 5, we ask whether devices at the levels of perfection required to exhibit three-state quantum coherent behaviour are possible, or indeed practical, to make by using deterministic doping methods. Our answer is very clearly positive. Although demonstrating CTAP is an important outcome for solid-state quantum information, its demonstration will also highlight the levels of control that are possible, and open new vistas for small quantum information processing tasks.

CTAP is an example of a three-site quantum protocol and has motivated a considerable amount of interest in the solid-state and atom-optical communities. Indeed, two independent and similar proposals for the entirely spatial analogue of the well-known stimulated Raman adiabatic passage (STIRAP) [16] protocol appeared almost simultaneously for atomic transport through three wells [17], and electronic transport through a line of donors or quantum dots [11]. Many of the theoretical studies in the atomic case have looked at sensing and inherent nonlinearities that can be achieved using Bose–Einstein condensates [18–20], whereas the solid-state investigations have considered feasibility [21–23], protocols and novel geometries [24–28]. Additionally, there has been progress towards realizing three-state systems in a range of triple-dot systems [29–34]. Although there is yet to be a demonstration with massive particles, three-waveguide structures have been proposed [35, 36], and these were demonstrated to exhibit photonic CTAP [37], straddling CTAP [38] and continuum CTAP [39]. In addition to the systems mentioned above, CTAP has also been proposed in Cooper–Pair box arrays [40] and spin chains [41]. These previous works provide motivation for the present paper to assess the precision of practical fabrication methods to construct arrays of single atoms for devices to implement CTAP in the solid state.

This paper is organized as follows. In section 2, we review CTAP and introduce new adiabatic results that allow quick determination of timescales for CTAP in experimentally important solid-state geometries. In particular, we focus on efficient methods to determine the total time required for a CTAP operation in a manner compatible with the architectures we envisage. Next, in section 3, we describe the development of our deterministic doping strategy that employs ion implantation through scanned nano-scale apertures. In section 4, we discuss the feasibility of employing this strategy to fabricate CTAP test devices. Finally, in section 5, we present exemplary simulations highlighting particular implanted donor configurations and conditions necessary to demonstrate high-fidelity CTAP using these devices. The combined results of these analyses is a critical evaluation of implantation strategies for CTAP devices, and an analysis of the probability of fabricating a working CTAP device based on the known limitation of the spatial precision of ion implantation imposed by straggling.

2. CTAP and adiabaticity

CTAP is a protocol for the spatial transport of a particle between two points on a quantum chain. In its simplest case, this is a three-site protocol with the central chain being a single site. CTAP is distinguished from STIRAP in that the variations in nearest-neighbour tunnel matrix elements (TMEs) are effected by direct modulation of the wave-function overlaps by either surface gate control [42] or well proximity [17]. Within the STIRAP approach, the TMEs are strictly electromagnetic field driven[2] and are commonly best considered as manipulation of excitations, rather than true particle transport as is the case for CTAP.

[2] However, we note that STIRAP across a spatial degree of freedom has been proposed in, for example, [43].

CTAP has certain advantages over competing transport mechanisms when applied to the task of scalable quantum computing in phosphorus in silicon (Si:P), and these have been thoroughly discussed in [13]. Briefly, at the required donor spacings for Si:P architectures, TMEs can be as large as 1 THz (at 20 nm interdonor spacing). Non-adiabatic control of such TMEs would require bandwidths at least an order of magnitude greater than this, which is clearly unfeasible for electrical control at base temperatures of dilution fridges. Hence, a sequential, non-adiabatic 'bucket brigade' scheme is not possible as a route to long-range transport. Another limitation with the original Kane approach to Si:P quantum computing [44] was the limitation of overall gate density that could be achieved in the on-chip control electronics [45, 46]. Extensions of CTAP to many donors (i.e. $\gg$3) via the straddling scheme [11], and to a lesser extent the alternating scheme [27], allow a reduction in the overall gate density by reducing the number of independent control gates required for long-range transport. Such gate density reductions are not available in either the non-adiabatic 'bucket brigade' approach or the adiabatic following technique discussed by Taylor *et al* [47]. Although the advantages of long-range CTAP through chains comprising many donors are not the subject of this work, successful demonstration of CTAP across a three-donor chain is a necessary milestone towards demonstrating the advantages of the long-range chains.

The CTAP pathway requires the adiabatic transformation of a particular electron eigenstate along a defined path in phase space. In the spatial setting, we restrict the control parameters to the tunnel matrix elements that are set by surface electrodes (gates), analogous to the way in which electromagnetic field intensities are varied in STIRAP. Although the device shown in figure 1(a) is yet to be made, it is the purpose of this paper to investigate potential fabrication methods based on currently available technologies. Devices of comparable complexity have been fabricated using the counted-ion implantation techniques described in [5], and we also note the demonstration of triple dots in GaAs 2DEG structures [29, 48, 49] and gated carbon nanotubes [31].

In order that transport may be effected in timescales short compared with the expected decoherence times, the donors need to be relatively close to each other. Ideally the device should comprise three donor atoms spaced 20–30 nm apart, 20 nm below the surface. Here we model departures from the ideal configuration imposed by the limitations of the implantation of ions through nano-scale apertures. We employ SRIM [50] Monte Carlo simulations to model the straggling of implanted ions into the substrate. The SRIM data in figures 1(c) show the probability distribution of 100 000 14 keV P^+ ions implanted through circular apertures 10 nm in diameter and centred on the desired atom locations. A phosphorus ion accelerated to 14 keV will travel around 23 nm into the substrate before stopping but can straggle away from this median position as it undergoes collisions with the Si lattice, giving the range distribution a standard deviation of 11 nm. A less energetic 7 keV ion will penetrate 14 nm below the surface and has 40% less straggle.

To model devices containing atoms implanted in this way, we begin by writing down the Hamiltonian of the three-donor one-electron problem in the three-state approximation where we only keep the lowest state of the electron localized around the donor.

Although we will later treat the next-nearest neighbour tunnelling as a potential noise limit, for the discussion that follows, it will be assumed to be zero. The CTAP protocol requires tuning of the energies of the sites so that they are equal. This is achieved by the surface gates S_1, S_2 and S_3 in figure 1(a). The adiabatic pathway is affected by modulating the barrier gates B_{12} and B_{23}. In practice, all gates will affect all of the relevant parameters, and so some cross compensation

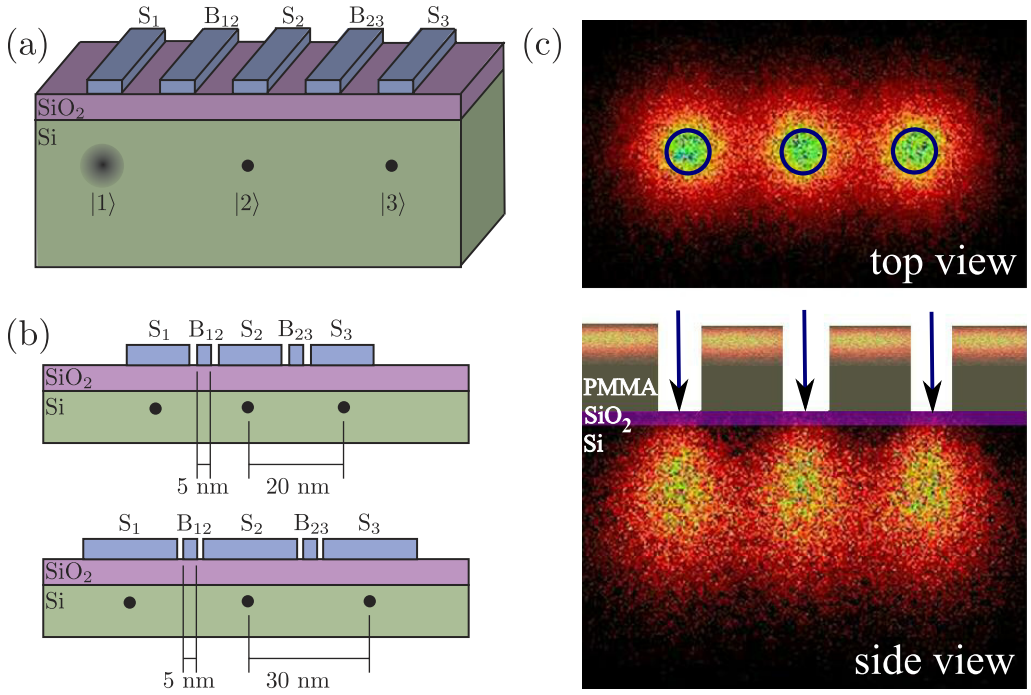

Figure 1. (a) Triple dopant, one-charge system with surface gate control for CTAP. The symmetry gates S_1 and S_3 maintain the degeneracy of the end of chain states, whereas the variations in the TMEs are effected by the barrier gates B_{12} and B_{23}. (b) For the greatest chance of producing a working device, 5 nm B gates will be required. They would be laid in the space left by the S gates. Spacings of 20 and 30 nm were used as the extrema of the nominal range. (c) *Top view* and *side view* of SRIM simulations (see text) showing the spatial probability distribution of 100 000 14 keV P^+ ions implanted into silicon through three apertures 10 nm in diameter and spaced 30 nm apart, patterned in 180 nm of PMMA. There is a 5 nm oxide present on the Si surface.

will be required [23], which can be determined by studying the three-dimensional charging diagram of the three-site system [29, 51]. Using the basis $|1\rangle$, $|2\rangle$, $|3\rangle$ with onsite energies $E_i = 0$ and TMEs $\Omega_{12}(t)$, $\Omega_{23}(t)$ and Ω_{13}. The Hamiltonian is

$$\mathcal{H}(t) = \Omega_{12}(t)|2\rangle\langle 1| + \Omega_{23}(t)|3\rangle\langle 2| + \Omega_{13}(t)|3\rangle\langle 1| + \text{h.c.}, \tag{1}$$

and with $\Omega_{13}(t) = 0$, the eigenstates are

$$|\mathcal{D}_0\rangle = \frac{\Omega_{23}|1\rangle - \Omega_{12}|3\rangle}{\sqrt{\Omega_{12}^2 + \Omega_{23}^2}}, \tag{2}$$

$$|\mathcal{D}_\pm\rangle = \frac{\Omega_{12}|1\rangle \pm \sqrt{\Omega_{12}^2 + \Omega_{23}^2}|2\rangle + \Omega_{23}|3\rangle}{\sqrt{2\left(\Omega_{12}^2 + \Omega_{23}^2\right)}}, \tag{3}$$

with energies

$$E_0 = 0, \tag{4}$$

$$E_\pm = \pm\sqrt{\Omega_{12}^2 + \Omega_{23}^2}. \tag{5}$$

The CTAP protocol can now be understood quite simply. The idea is to remain in the state $|\mathcal{D}_0\rangle$ and to vary the TMEs so that at time $t = 0$ the system is in the desired initial state, e.g. $|\mathcal{D}_0(t = 0)\rangle = |1\rangle$, and at time $t = t_{\max}$ the system is in the desired final state, e.g. $|\mathcal{D}_0\,(t = t_{\max})\rangle = |3\rangle$. Note that although this three-mode description for the tunnelling is obviously a simplification, it still captures all of the essential physics of the CTAP protocol, a fact confirmed by recent analyses of CTAP in the triple square well case [21, 22] and atomistic simulations of the ideal case [23]. It is also interesting to note another point of distinction between STIRAP and CTAP. Transport in STIRAP also employs the adiabatic following described above, but there is another mechanism that acts to improve the fidelity of the transport: coherent population trapping. In the case of STIRAP, $|\mathcal{D}_0\rangle$ is also the *dark state*, i.e. a state decoupled from the driving fields and also from spontaneous emission. Any leakage of population out of the dark state, e.g. caused by varying the Hamiltonian too quickly, is therefore optically pumped back into the dark state. In this way, spontaneous emission actually serves to improve the fidelity of the STIRAP mechanism. This channel is not, in general, open to CTAP because at the temperatures and energy scales necessary for CTAP in Si:P, there is not expected to be any appreciable T_1 relaxation from the middle site into the other states.

To effect CTAP, there is clearly a large amount of flexibility to choose the pulsing scheme for the TMEs. In STIRAP protocols, Gaussian or Gaussian-like pulses are most commonly employed because of the necessity to turn on the excitation (laser pulse) before varying it [16]. However, in the solid state, where nonzero TMEs arise solely due to donor proximity, such a pulsing is not required, and so we advocate the use of the pulses that vary between their extrema at $t = 0$ and $t_{\max}$. Such pulses are explicitly stated below and illustrated in figure 2, and they are chosen to be sinusoidal for analytical convenience. In [20, 26, 52] error function pulses were employed, which have some advantages in terms of smoothness of evolution and in nonlinear systems avoid certain complications due to eigenstate degeneracy at the ends of the protocol. It should be noted that the TMEs between sites vary exponentially with applied gate voltage [42] and so, although the TMEs are varied sinusoidally, the form of the control biases will differ [21].

To determine whether the system remains in the target state, we invoke the adiabaticity criterion, and due to symmetry we define (without loss of generality) the adiabaticity parameter to be between $|\mathcal{D}_0\rangle$ and $|\mathcal{D}_+\rangle$. The adiabaticity parameter can be defined as

$$\mathcal{A} \equiv \frac{\langle \mathcal{D}_+ | \frac{\partial \mathcal{H}}{\partial t} | \mathcal{D}_0 \rangle}{|E_+ - E_0|^2}, \tag{6}$$

and for adiabatic evolution we require $\mathcal{A} \ll 1$. Note that this is equivalent to other means of quantifying the adiabaticity, e.g. that given in [16]. One should be mindful of the fact that the adiabaticity does not translate to a direct measure of fidelity; it is rather a measure of when the assumption of adiabatic evolution is justified. Choosing as the form for the surface gate controlled TMEs

$$\Omega_{12}(t) = W_{12} \sin^2\left(\frac{\pi t}{2t_{\max}}\right), \tag{7}$$

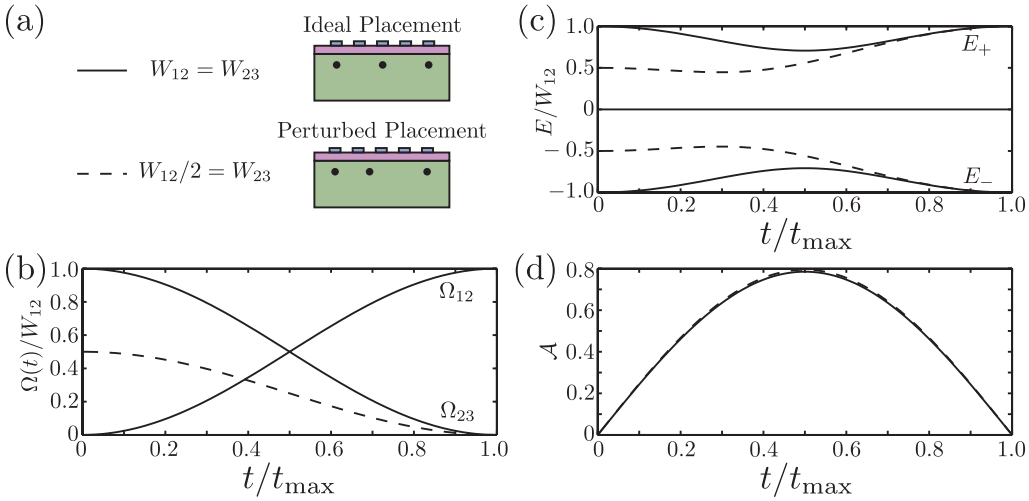

Figure 2. (a) Two of the many possible scenarios for three implanted donors, where they are equally spaced and where the right spacing is half the left. (b) TMEs as a function of time. The solid lines correspond to the case that $W_{12} = W_{23}$ for the sinusoidal variation as defined in the text, whereas the dashed line corresponds to the case that $W_{23} = W_{12}/2$. (c) Eigenenergies of the states as a function of time with the sinusoidal variation; again the solid lines are for $W_{12} = W_{23}$ and the dashed line for $W_{23} = W_{12}/2$. (d) The value of the adiabaticity parameter $\mathcal{A}$ throughout the process. Note that it is maximized at $t = t_{\max}/2$ irrespective of the values of W_{12} and W_{23}, although there are minor differences in the value of $\mathcal{A}$. As expected, the process is slightly less adiabatic with the smaller values of W.

$$\Omega_{23}(t) = W_{23} \cos^2\left(\frac{\pi t}{2t_{\max}}\right) \tag{8}$$

gives

$$\mathcal{A} = \frac{\pi W_{12} W_{23} \sin(\pi t/t_{\max})}{\sqrt{2} t_{\max} \left(W_{12}^2 + W_{23}^2\right)^{3/2}}. \tag{9}$$

It is important to note here that the adiabaticity is a maximum when $t = t_{\max}/2$ irrespective of the relative values of W_{12} and W_{23}. This is significant in the design of robust sequences and in affording a quick estimate of the required timescale for CTAP operation on devices fabricated subject to the statistical variations of ion implantation. To illustrate the energies, TMEs and adiabaticity, in figure 2 we present characteristic plots for the case that $W_{12} = W_{23}$ and when $W_{23} = W_{12}/2$.

In a realistic experiment, we will set the time for CTAP, given a certain desired adiabaticity. Hence it is more important to rearrange (9) to determine the value for $t_{\max}$ that keeps the maximum value of $\mathcal{A}$ at or below some threshold, i.e. we determine

$$t_{\max} = \frac{\pi W_{12} W_{23}}{\sqrt{2}\mathcal{A} \left(W_{12}^2 + W_{23}^2\right)^{3/2}}, \tag{10}$$

where we have dropped the sine term because we are evaluating $t_{\max}$ with respect to the maximum value of $\mathcal{A}$. Equation (10) is particularly useful in gaining insight into the

practicalities of CTAP. The most obvious impediment to very long timescales will be the limits placed by decoherence, which will set a maximum length of time over which the protocol can be conducted [11, 53, 54].

Until now we have neglected the next-nearest-neighbour tunnelling, i.e. Ω_{13}. Formally, there is no CTAP pathway for nonzero Ω_{13} as the Hamiltonian (1) has no null (or dark) state; however, we can place a good bound on whether neglecting Ω_{13} will be valid by comparing the period for oscillation on the $|1\rangle - |3\rangle$ transition directly, with the total time for CTAP. We introduce $\mathcal{J} \equiv \Omega_{13} t_{\max}$ and assert that if $\mathcal{J} \ll 1$, then we may ignore the effect of Ω_{13} in our analysis. This criterion is helpful for proof of concept devices, but may not suffice to assess applicability for a large-scale quantum computer where more rigorous error control is required [13]. Having now established the criteria for successful operation of a CTAP device, we now turn to the practicalities of fabrication.

3. Deterministic doping using nano-apertures

Although ion implantation is an industry-standard technique for the introduction of dopant atoms into semiconductor materials, there are three main limitations to applying the technique to deterministic doping: the registration of individual ion strikes, spatial registration of the ion implant site and straggling of the ion due to the statistical nature of the stopping process.

We propose here that these problems are now close to being solved to the level required for the fabrication of a prototype three-atom CTAP device. The first problem has several demonstrated solutions. These include registration of individual ion strikes by on-chip detector electrodes [5]; changes in the source–drain current in MOSFETs or micro-resistors [6, 55]; or detection of the secondary electrons liberated from the surface of the substrate [6]. To overcome the second problem, regarding spatial registration of the ion impact, these methods have been combined with either surface masks written on the device surface with electron beam lithography (EBL) or the use of a sub-100 nm focused ion beam [15]. A further alternative is the use of a scanned nano-aperture to collimate the ion beam. Use of a nano-aperture in the cantilever of an atomic force microscope (AFM) has demonstrated a spatial precision of 90 nm [56] with the potential of a few nm in the near future.

For the present paper, we will concentrate on a deterministic doping system that we are developing to fabricate the structures described in the previous section. However, the system can be used for other ions and other energies because no special ion source is required to achieve the spatial resolution. Our system implants single ions collimated by a scannable nano-aperture as in the conceptual schematic shown in figure 3. Ion strike registration by on-chip detector electrodes has already been demonstrated [5]. Briefly, this method employs LN_2 cooling of the substrate and a charge-sensitive JFET preamplifier provides low enough noise to detect the charge induced by the impact of a single ion into the substrate. We present here proof of principle experiments with the most important elements of this system, in particular our ability to deliver single ions to specific locations on the substrate. Here we employ 500 keV He^+ ions for simplicity—these ions can be detected at room temperature with a test substrate consisting of a commercial photodiode.

Our nano-aperture has been fabricated in a 2.5 μm-thick Si cantilever using a focused ion beam (FIB) system using the method of Schenkel *et al* [57]. An initial slot is milled with the FIB, which is backfilled by the *in situ* deposition of Pt dissociated from a precursor gas by the ion beam. Slots fabricated in this way were typically down to about 60 nm in width in the

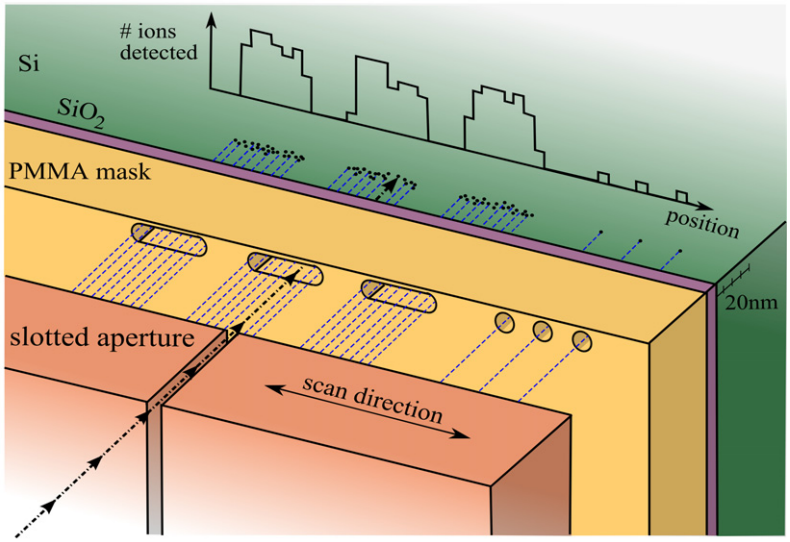

Figure 3. Schematic of the scanned nano-aperture apparatus. A cantilever drilled with a perpendicular slot is scanned parallel to a one-dimensional array of static surface apertures patterned in PMMA with EBL. First, the position of the scanned aperture is registered by detecting ions in a registration zone. Once the position of the aperture has been identified, deterministic implants can be performed in the implant zone.

2.5 μm thickness of the cantilever, which is sufficient to mask a 500 keV He^+ ion. We have used an aperture nominally 100 nm wide and 10 μm long onto which was directed the incident 500 keV He^+ ion beam focused to a 1 μm spot as described in [58].

The substrate that received the implant was a Hamamatsu S1223 photodiode mounted on a Nanonics piezoelectric scanning stage. The surface of the photodiode was masked with a test structure fabricated in a spin-coated 0.4 μm PMMA and patterned with EBL to produce trenches that reached the substrate as shown in the AFM topographical image in figure 4. In this experiment, the slot in the cantilever was oriented parallel to the trenches. The substrate was then scanned in the perpendicular direction for both 220 and 28 nm steps. The spectrum of ion energy collected from the charge induced by ion impacts in the substrate was recorded at each step.

Features of the resulting ion energy spectra show signals at low energy from ions that enter the substrate after losing energy from passing through the full thickness of the PMMA mask surrounding the trenches. Signals corresponding to the incident beam energy are from ions that impact the substrate directly through a trench. A map of the ion intensity as a function of ion energy loss and cantilever step position produces the images shown in figures 4(a) and (c). These images faithfully represent the two-dimensional structure of the PMMA film when compared to the AFM trace in figures 4(b) and (d) and confirm the function of the system with a nominal spatial resolution of 100 nm, which is expected from the width of the nano-aperture.

We also conclude that not all ions are transmitted through the nano-aperture with full energy, as some ions forward scatter from the walls of the aperture and this can be seen from the low-energy signals. However, for the proposed application of the system to implant sub-14 keV ions, the nano-aperture can be made in a much thinner substrate, which will allow

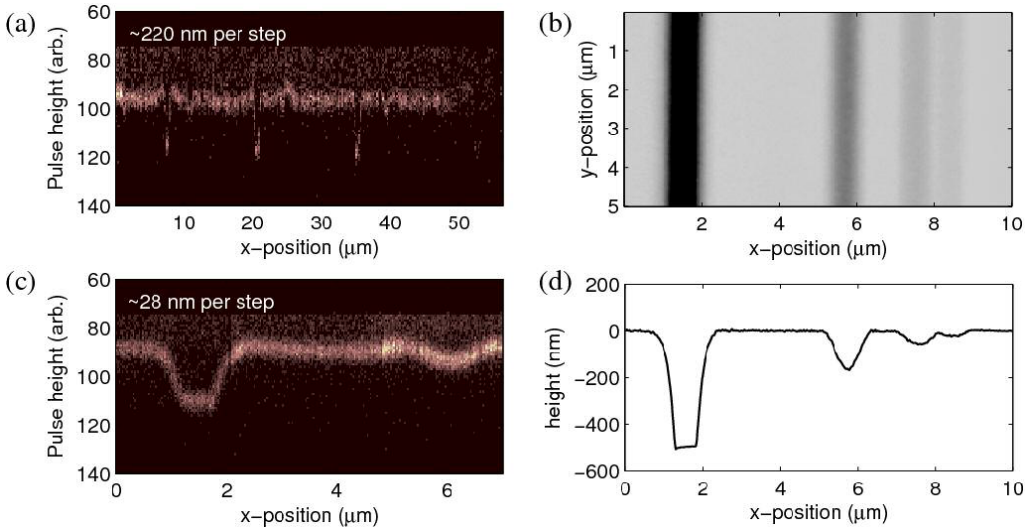

Figure 4. (a) The ion impact pulse height (energy signal) from the photodiode substrate as a function of the position of the scanned nano-aperture with a step size of 220 nm. The colour scale represents the intensity of ions at a given energy. (b) AFM image of the patterned PMMA. (c) The same as (a) but with a step size of 28 nm. (d) Trace from the AFM image of the patterned PMMA.

narrower apertures to be made [59–61], and ions scattered in the aperture will be unable to enter the substrate except through the open areas of the PMMA mask. When applied to fabricate a deterministically doped device, the stepping of the cantilever would be gated on the ion impact signals, thus delivering a single implanted atom to each site.

4. Implications for ion-implanted devices

Now we are in a position to evaluate the use of our deterministic doping system demonstrated here to calculate the *theoretical* yield of three-donor CTAP test devices. We use an appropriate Hamiltonian following the theory of section 2 and employ the SRIM Monte Carlo simulations of the ion straggling. We also restrict ourselves to the hydrogenic approximation, which is the only computationally feasible method for simulating a large number of devices to evaluate the statistical variations in the straggling process. This should be contrasted with the more accurate, but substantially more computationally intensive rigorous identification of the CTAP pathway in an ideal three-donor device using the atomistic NEMO3D package [23].

To determine the bare (unperturbed) TMEs, we use the hydrogenic approximation [62, 63] applied by Openov [64] as a simplified approach to the study of singly ionized double-donor structures [65, 66]. These results are applicable to donor separations predominantly along the [100] direction in silicon where the valley degeneracy has less effect [10, 65, 67, 68].

We use

$$W_{ij} = 4E^* \left(\frac{d_{ij}}{a_B^*}\right) \exp\left(-\frac{d_{ij}}{a_B^*} - 1\right), \tag{11}$$

where E^* is the effective Hartree energy and d_{ij} is the interdonor separation between donors i and j. With these constraints, we can immediately write down $t_{\max}$ and $\mathcal{J}$ as

$$t_{\max} = \frac{\pi a_B^* d_{12} d_{23} \exp\left(-(d_{12}+d_{23})/a_B^* - 2\right)}{4\sqrt{2}E^* \mathcal{A}\left[(F_{12})^2 + (F_{23})^2\right]^{3/2}}, \tag{12}$$

$$\mathcal{J} = \frac{\pi d_{12} d_{23} d_{13} \exp\left(-(d_{12}+d_{23}+d_{13})/a_B^* - 3\right)}{\sqrt{2}\mathcal{A}\left[(F_{12})^2 + (F_{23})^2\right]^{3/2}}, \tag{13}$$

$$F_{ij} = d_{ij} \exp\left(-\frac{d_{ij}}{a_B^*} - 1\right) = \frac{W_{ij} a_B^*}{4E^*}. \tag{14}$$

A rigorous calculation of $t_{\max}$ and $\mathcal{J}$ would involve full band structure considerations, but these formulae give an extremely efficient mechanism for determining these important parameters with relatively minimal computational cost. The hydrogenic approximation of equation (11) also allows us to determine the fraction of simulated devices that have tunnelling rates W_{ij} larger than the valley–orbit splitting (10.8 meV) to the 1s excited states. Taking the simple gate geometry shown in figure 1(a), we can exclude implanted donors that prohibit the placement of a 5 nm gate between them which will prevent control of the tunnelling rates.

Additionally, donors too close to the surface may hybridize with states at the oxide interface [69–71]. While this may not necessarily be a catastrophic failure channel, we will exclude ion arrays where one or more of the donors are closer than 5 nm to the interface as the coherence times are expected to be shorter and the approximation assumed in our CTAP analysis is expected to be not valid. Donors deeper than 25 nm are expected to be difficult to control with reasonable surface gate potentials; hence we identify this as another failure mode.

To explore the statistical variations in possible three-donor devices, we performed SRIM simulations of the straggling for both 14 and 7 keV P^+ implants where the ion strike location was chosen randomly within one selected aperture in a three-aperture array. Each aperture was assumed to be 10 nm in diameter (state-of-the-art for EBL in PMMA), separated linearly by either 20 or 30 nm. 14 keV P^+ ions reach an average depth of 23 nm below the substrate surface and it is therefore possible to implant through a typical 5 nm gate oxide employing the demonstrated on-chip detector electrodes [5]. Simulations for the 7 keV P^+ ions assume a state-of-the-art 1.2 nm gate oxide and will achieve a higher placement precision because the effect of lateral and longitudinal straggle will be less. Near-future developments of the on-chip detection system to improve sensitivity may allow the deterministic implant of 7 keV P^+ ions.

The results of our simulations are shown in figure 5 and table 1. For each three-donor array, in which the donor positions vary according to the statistics and the randomly selected impact site within the corresponding aperture, we have calculated Δ_{SAS}, $t_{\max}$ and $\mathcal{J}$. For a donor spacing of 20 nm, the straggle of implanted ions is more detrimental to the control requirements than to the coherence restrictions. When the donor implantation spacing is increased to 30 nm, the lateral straggle affecting gate control is less important while the portion of donors with $t_{\max} < 10$ ns decreases. One in nine devices fabricated with 14 keV P^+ implants into the 10 nm apertures spaced 20 nm apart will have suitable configurations, while the implants into the same apertures spaced 30 nm apart increase the yield to one in six. Decreasing the energy of the phosphorus ion to 7 keV increases this to better than one in two devices with favourably placed ions.

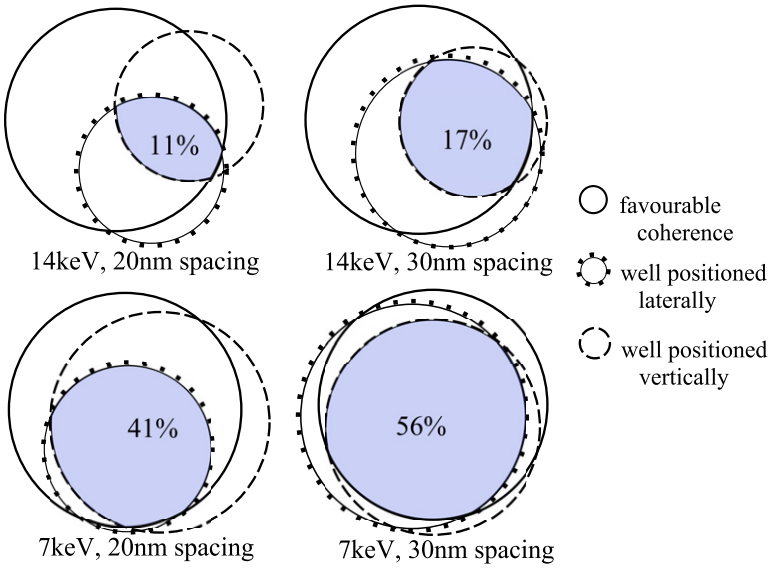

Figure 5. The overlap of success modes in a given three-donor array. In the 14 keV, 20 nm spacing Venn diagram, most arrays with a short enough $t_{\max}$, small $\mathcal{J}$, suitable Δ_{SAS} or $d_{13} > d_{12}/d_{23}$ (favourable coherence) are also suitably positioned for alignment with the surface gates (well positioned laterally) and/or for suitable gate control (well positioned vertically). Increasing the implant spacing to 30 nm subtly decreases the total number of arrays that have sufficiently short $t_{\max}$ times but greatly increases the number of arrays that are well positioned laterally, and this increases the number of successful arrays to one in six.

5. Device simulations

The calculations of Δ_{SAS} using the hydrogenic approximation above do not take into account factors such as device geometry and the physics of the silicon substrate. To gain further insight and confirm the criteria specifying *geometrically* suitable triplets have suitable pairwise Δ_{SAS}, more accurate methods are required, which we perform here on selected simulated devices. From the large number of configurations in the simulations of the previous section, we select a number of donor configurations that are to be on the border of suitability and perform a calculation of the gate-controlled pairwise tunnelling rates. We model the gate potentials by employing the industry-standard semiconductor device modelling code ISE-TCAD (see [72]).

We model a simplified structure consisting of two donors buried in silicon with one barrier gate between them to modulate the tunnelling rate. For these calculations, we use the same approach applied in [27] using a finite element modelling package to simulate the electric potential in the device in response to different applied barrier gate biases. These simulations are then in turn used in a Monte Carlo calculation of the Hamiltonian for the pair of donors, modelling the barrier gate as an infinite line of charge. We extract the electric potential within the device at mesh points from the finite element modelling simulations and fit a linear charge density that would give rise to the same potential landscape resulting in an expression for the electric potential due to the gate bias to include in the Monte Carlo calculation. This approach allows for any gate bias to be used, and yields the electric potential at any point in the space of

Table 1. Percentage of three-donor devices that satisfy control or coherence restrictions with our present model including straggling. The success modes are listed for implanted donors that are implanted P^+ ions with energies of either 7 or 14 keV at a randomly selected impact site within three 10 nm diameter apertures spaced either 20 or 30 nm apart. An array of three donors needs to satisfy all placement conditions to be considered viable (see figure 5); the percentage of three-donor arrays that satisfy *all* control and coherence requirements is given for each implant scenario.

	20 nm spacing		30 nm spacing	
Success mode	14 keV (%)	7 keV (%)	14 keV (%)	7 keV
$\mathcal{J}_{\max} < 0.001$	97	98	99	100%
$t_{\max} < 10$ ns	95	100	84	91%
$\Delta_{SAS} < 10.8$ meV	95	95	99	100%
$d_{13} > d_{12}, d_{23}$	83	87	96	100%
Not too shallow >5 nm	72	75	72	75%
Not too deep <25 nm	42	90	42	90%
Lateral separation >gate width	34	63	62	90%
CTAP suitable arrays	11	41	17	56

the calculation without the need for recalculating the device potential for each bias separately using the ISE-TCAD package, and without having to interpolate between the mesh points used by the simulation to obtain the potential for an arbitrary point in the Monte Carlo calculation.

The Hamiltonian for the two-donor, Si:P system is written as

$$\mathcal{H} = \mathcal{H}_{Si} + V_d(r - R_1) + V_d(r - R_2) + V_E, \tag{15}$$

where $\mathcal{H}_{Si}$ is the Hamiltonian of an electron in the pure silicon lattice, which includes both a kinetic term and the effective potential due to the silicon lattice; V_d is the Coulombic potential of each donor, located at the coordinates R_1 and R_2; and V_E is the field applied externally through the barrier gate [68, 73, 74].

The Monte Carlo simulation was first applied to an ideal system closely modelled on the 14 keV P^+ implantation example. In this case, the implanted donors were assumed to be 'perfectly' aligned with spacing 20 nm apart, exactly symmetrically about a 5 nm wide gate and buried 20 nm below the oxide–silicon interface, as is shown in figure 6(a). This was then compared with the same simulation run for donors spaced 2.5 and 15 nm on either side of the centreline of the gate and 20 nm deep, shown in figure 6(b).

By the geometric conditions imposed in section 4, these configurations would be deemed to be just within the bounds of being part of a functional three-donor CTAP device. The resulting gate voltage bias to find the Δ_{SAS} for each of these pairs of donors is shown below. Figure 7 shows the results for varying the lateral alignment of the donors.

For the perfect alignment case, we obtain a minimum gate varied tunnelling rate of $\sim 1\,\mu$eV and may be driven from this minimum up to $\sim 100\,\mu$eV with a change of less than 100 mV in the barrier gate voltage. When we investigate a pair with disorder in the lateral coordinate, we see that the lateral misalignment results in a minimum gate modulated tunnelling rate higher than that for the perfectly aligned pair.

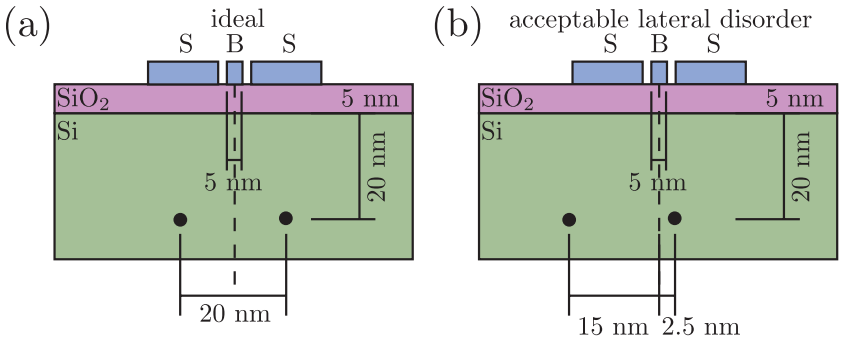

Figure 6. Configurations of donor pairs calculated. (a) The 'perfect' alignment example. (b) Donor pair with lateral disorder at the limits of the geometrically acceptable bounds.

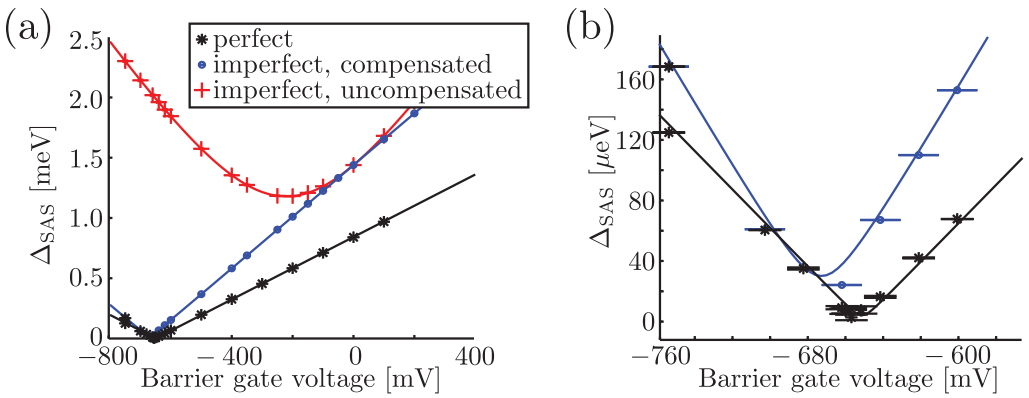

Figure 7. (a) Δ_{SAS} curves for donors perfectly aligned, misaligned in the lateral coordinate and misaligned but setting v_z to 0 to simulate the resultant Δ_{SAS} when the misalignment is completely compensated. Errors are due to the numerical errors from the Monte Carlo routine. (b) Close-up of the anti-crossings for the ideal and compensated imperfect cases near zero TME.

Figure 8 shows the v_x and v_z components of the Hamiltonian. These are coefficients of the Pauli matrices σ_x and σ_z of the external field component of the Hamiltonian after a Pauli decomposition has been performed, with donors laterally separated along the x-direction. To suppress the tunnelling (or at least decrease the Δ_{SAS} by two orders of magnitude), another gate must be used to compensate for the misalignment. This gate would need to provide a voltage to oppose the v_z component of the Hamiltonian that arises from this asymmetry.

These results show that such a pair on the boundary of the geometric criteria in lateral disorder does in fact yield a Δ_{SAS}, and suppression of the tunnelling rate can be achieved with a change of gate bias of order only 100 mV, compatible with that required for the CTAP protocol. In this hydrogenic model, the depth straggle case is difficult to model and awaits further developments of the theory.

6. Conclusions

The construction of proof-of-principle devices, for CTAP in particular, requires the ability to accurately place donors within a substrate. We have experimentally demonstrated some aspects

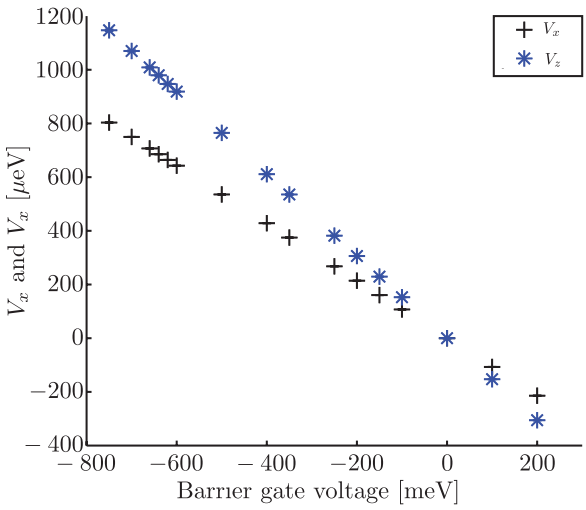

Figure 8. Components of the two-donor Hamiltonian as a function of the barrier gate voltage (v_x and v_z). To suppress Δ_{SAS} one must be able to vary v_x to cancel with the bare Si:P-P+ h_x and for v_z to be close to zero or at least smaller by an order of magnitude than v_x so as not to dominate the Δ_{SAS} calculation. From the plot we see that for the pair with disorder in their lateral separation, the v_z component is comparable with v_x. This suggests that it may reasonably be compensated using another surface gate.

of just such a method of implanting single ions deterministically. We have also simulated ion-implanted three-donor CTAP devices using SRIM to model the lateral straggling within the constraints of a realistic fabrication system to assess the impact of finite accuracy. In our analysis, we have not gone beyond the hydrogenic approximation to donor interaction (which can be done with NEMO3D [23, 75]), as atomistic approaches are far too numerically intensive to explore the very large number of configurations investigated here.

However, our results suggest that a yield of successful devices of better than one in six is immediately realizable with 14 keV phosphorus ion implantation, improving to one in two with the near future innovation of 7 keV ion detection. Such yields are certainly adequate for proof-of-concept devices. Numerical modelling of devices with greatest allowable lateral disorder confirms that tunnelling can be controlled with reasonable gate voltages.

The study highlights the need to improve the deterministic doping technique to allow implants at lower energies for more accurate placement, provided also that issues associated with the proximity of the oxide can also be ovecome. The prospect of scaling up to longer CTAP chains required for large-scale quantum computer architectures [13] is expected to be less favourable, and hydrogen-resist lithography methods for producing such CTAP chains may be required. On the basis of our results, however, we predict that ion implantation is a viable route to the fabrication of proof-of-concept CTAP devices with three atoms.

Acknowledgments

ADG is the recipient of an Australian Research Council Queen Elizabeth II Fellowship (project number DP0880466). LCLH is the recipient of an Australian Research Council

Australian Professorial Fellowship (project number DP0770715). This work was supported by the Australian Research Council Centre of Excellence for Quantum Computer Technology, the Australian Government and the US National Security Agency (NSA) and the Army Research Office (ARO) under contract number W911NF-08-1-0527.

References

[1] The International Technology Roadmap for Semiconductors http://www.itrs.net
[2] A Quantum Information Science Technology Roadmap 2004 http://qist.lanl.gov/pdfs/qc_roadmap.pdf
[3] Ruess F J, Oberbeck L, Simmons M Y, Goh K E J, Hamilton A R, Hallam T, Schofield S R, Curson N J and Clark R G 2004 Toward atomic-scale device fabrication in silicon using scanning probe microscopy *Nano Lett.* **4** 1969–73
[4] Persaud A, Park S J, Liddle J A, Schenkel T, Bokor T and Rangelow I W 2005 Integration of scanning probes and ion beams *Nano Lett.* **5** 1087
[5] Jamieson D N *et al* 2005 Controlled shallow single-ion implantation in silicon using an active substrate for sub-kev ions *Appl. Phys. Lett.* **86** 202101
[6] Shinada T, Kurosawa T, Nakayama H, Zhu Y, Hori M and Ohdomari I 2008 A reliable method for the counting and control of single ions for single-dopant controlled devices *Nanotechnology* **19** 345202
[7] Meijer J *et al* 2006 Concept of deterministic single ion doping with sub-nm spatial resolution *Appl. Phys. A: Mater. Sci. Process.* **83** 321–7
[8] Hanssen J L, Hill S B, Orloff J and McClelland J J 2008 Magneto-optical-trap-based, high brightness ion source for use as a nanoscale probe 2008 *Nano Lett.* **8** 2844–50
[9] Schnitzler W, Linke N M, Fickler R, Meijer J, Schmidt-Kaler F and Singer K 2009 Deterministic ultracold ion source targeting the Heisenberg limit *Phys. Rev. Lett.* **102** 070501
[10] Hollenberg L C L, Dzurak A S, Wellard C, Hamilton A R, Reilly D J, Milburn G J and Clark R G 2004 Charge-based quantum computing using single donors in semiconductors *Phys. Rev.* B **69** 113301
[11] Greentree A D, Cole J H, Hamilton A R and Hollenberg L C L 2004 Coherent electronic transfer in quantum dot systems using adiabatic passage *Phys. Rev.* B **70** 235317
[12] Schofield S R, Curson N J, Simmons M Y, Rueß F J, Hallam T, Oberbeck L and Clark R G 2003 Atomically precise placement of single dopants in Si *Phys. Rev. Lett.* **91** 136104
[13] Hollenberg L C L, Greentree A D, Fowler A G and Wellard C J 2006 Two-dimensional architectures for donor-based quantum computing *Phys. Rev.* B **74** 045311
[14] Sanders B C, Hollenberg L C L, Edmundson D and Edmundson A 2008 Visualizing a silicon quantum computer *New J. Phys.* **10** 125005
[15] Shinada T, Okamoto S, Kobayashi T and Ohdomari I 2005 Enhancing semiconductor device performance using ordered dopant arrays *Nature* **437** 1128–31
[16] Vitanov N V, Halfman T, Shore B W and Bergmann K 2001 Laser-induced population transfer by adiabatic transfer techniques *Annu. Rev. Phys. Chem.* **52** 763
[17] Eckert K, Lewenstein M, Corbalán R, Birkl G, Ertmer W and Mompart J 2004 Three-level atom optics via the tunneling interaction *Phys. Rev.* A **70** 023606
[18] Graefe E M, Korsch H J and Witthaut D 2006 Mean-field dynamics of a Bose–Einstein condensate in a time-dependent triple-well trap: nonlinear eigenstates, Landau–Zener models, and stimulated Raman adiabatic passage *Phys. Rev.* A **73** 013617
[19] Deasy K, Busch T, Niu Y, Gong S, Jin S and Chormaic S Nic 2006 Controlled creation of spatial superposition states for single atoms arXiv:quant-ph/0611174
[20] Rab M, Cole J H, Parker N G, Greentree A D, Hollenberg L C L and Martin A M 2008 Spatial coherent transport of interacting dilute bose gases *Phys. Rev.* A **77** 061602

[21] Cole J H, Greentree A D, Hollenberg L C L and Das Sarma S 2008 Spatial adiabatic passage in a realistic triple well structure *Phys. Rev.* B **77** 235418
[22] Opatrný T and Das K K 2009 Conditions for vanishing central-well population in triple-well adiabatic transport *Phys. Rev.* A **79** 012113
[23] Rahman R, Park S H, Cole J H, Greentree A D, Muller R P, Klimeck G and Hollenberg L C L 2009 Atomistic simulations of adiabatic coherent electron transport in triple donor systems *Phys. Rev.* B **80** 035302
[24] Greentree A D, Devitt S J and Hollenberg L C L 2006 Quantum-information transport to multiple receivers *Phys. Rev.* A **73** 032319
[25] Petrosyan D and Lambropoulos P 2006 Coherent population transfer in a chain of tunnel coupled quantum dots *Opt. Commun.* **264** 419–25
[26] Devitt S J, Greentree A D and Hollenberg L C L 2007 Information free quantum bus for generating stabiliser states *Quantum Inf. Process.* **6** 229
[27] Jong L M, Greentree A D, Conrad V I, Hollenberg L C L and Jamieson D N 2009 Coherent tunneling adiabatic passage with the alternating coupling scheme *Nanotechnology* **20** 5402
[28] Jong L M and Greentree A D 2010 Interferometry using spatial adiabatic passage in quantum dot networks *Phys. Rev.* B **81** 035311
[29] Schröer D, Greentree A D, Gadreau L, Eberl K, Hollenberg L C L, Kotthaus J P and Ludwig S 2007 Electrostatically defined serial triple quantum dot charged with few electrons *Phys. Rev.* B **76** 075306
[30] Xu K, Green J E, Heath J R, Remacle F and Levine R D 2007 *J. Phys. Chem.* C **111** 17852
[31] Grove-Rasmussen K, Jørgensen H I, Hayashi T, Lindelof P E and Fujisawa T 2008 Triple a quantum dot in a single-wall carbon nanotube *Nano Lett.* **8** 1055–60
[32] Gaudreau L, Sachrajda A S, Studenikin S, Kam A, Delgado F, Shim Y P, Korkusinski M and Hawrylak P 2009 Coherent transport through a ring of three quantum dots *Phys. Rev.* B **80** 075415
[33] Amaha S, Hatano T, Kubo T, Teraoka S, Tokura Y, Tarucha S and Austing D G 2009 Stability diagrams of laterally coupled triple vertical quantum dots in triangular arrangement *Appl. Phys. Lett.* **94** 092103
[34] Pierre M, Wacquez R, Roche B, Jehl X, Sanquer M, Vinet M, Prati E, Belli M and Fanciulli M 2009 Compact silicon double and triple dots realized with only two gates *Appl. Phys. Lett.* **95** 242107
[35] Paspalakis E 2006 Adiabatic three-waveguide directional coupler *Opt. Commun.* **258** 30–4
[36] Longhi S, Della Vale G, Ornigotti M and Laporta P 2007 Coherent tunneling by adiabatic passage in an optical waveguide system *Phys. Rev.* B **76** 201101
[37] Longhi S 2007 Light transfer control and diffraction management in circular fibre waveguide arrays *J. Phys. At. B: Mol. Phys.* **40** 4477–92
[38] Della Valle G, Ornigotti M, Toney Fernandez T, Laporta P, Longhi S, Coppa A and Foglietti V 2008 Adiabatic light transfer via dressed states in optical waveguide arrays *Appl. Phys. Lett.* **92** 011106
[39] Dreisow F, Szameit A, Heinrich M, Keil R, Nolte S, Tünnermann A and Longhi S 2009 Adiabatic transfer of light via a continuum in optical waveguides *Opt. Lett.* **34** 2405
[40] Siewert J and Brandes T 2004 Applications of adiabatic passage in solid-state devices *Adv. Solid State Phys.* **44** 1248–1249
[41] Ohshima T, Ekert A, Oi D K L, Kaslizowski D and Kwek L C 2007 Robust state transfer and rotation through a spin chain via dark passage arXiv:quant-ph/0702019
[42] Wellard C J, Hollenberg L C L, Parisoli F, Kettle L M, Goan H-S, McIntosh J A L and Jamieson D N 2003 Electron exchange coupling for single-donor solid-state spin qubits *Phys. Rev.* B **68** 195209
[43] Hohenester U, Troiani F, Molinari E, Panzarini G and Macchiavello C 2000 *Appl. Phys. Lett.* **77** 1864
Brandes T, Renzoni F and Blick R H 2001 *APhys. Rev.* B **64** 035319
Pazy E, D'Amico I, Zanardi P and Rossi F 2001 *Phys. Rev.* B **64** 195320
[44] Kane B E 1998 A silicon-based nuclear spin quantum computer *Nature* **393** 133
[45] Oskin M, Chong F T, Chuang I L and Kubiatowicz J 2003 Building quantum wires: the long and the short of it *Int. Symp. on Computer Architecture* p 374
[46] Copsey D, Oskin M, Impens F, Metodiev T, Cross A, Chong F T, Chuang I L and Kubiatowicz J 2003 Toward a scalable, silicon-based quantum computing architecture *IEEE J. Sel. Top. Quantum Electron.* **9** 1552–69

[47] Taylor J M, Engel H-A, Dür W, Yacoby A, Marcus C M, Zoller P and Lukin M D 2005 Fault-tolerant architecture for quantum computation using electrically controlled semiconductor spins *Nat. Phys.* **1** 177–83

[48] Gadreau L, Studenikin S A, Sachrajada A S, Zawadzki P and Kam A 2006 Stability diagram of a few-electron triple dot *Phys. Rev. Lett.* **97** 036807

[49] Rogge M C and Haug R J 2008 Two-path transport measurements on a triple quantum dot *Phys. Rev.* B **77** 193306

[50] Ziegler J F 2004 SRIM-2003 *Nucl. Instrum. Methods* B **219–220** 1027–36

[51] Rogge M C and Haug R J 2009 The three dimensionality of triple quantum dot stability diagrams *New J. Phys.* **11** 113037

[52] Greentree A D, Cole J H, Hamilton A R and Hollenberg L C L 2005 Scaling of coherent tunneling adiabatic passage in solid-state coherent quantum systems *SPIE Conf. Ser.* vol 5650 ed J-C Chiao, D N Jamieson, L Faraone and A S Dzurak, pp 72–80

[53] Ivanov P A, Vitanov N V and Bergmann K 2004 Effect of dephasing on stimulated Raman adiabatic passage *Phys. Rev.* A **70** 063409

[54] Kamleitner I, Cresser J and Twamley J 2008 Adiabatic information transport in the presence of decoherence *Phys. Rev.* A **77** 032331

[55] Batra A, Weis C D, Reijonen J, Persaud A, Schenkel T, Cabrini S, Lo C C and Bokor J 2007 Detection of low energy single ion impacts in micron scale transistors at room temperature *Appl. Phys. Lett.* **91** 193502

[56] Persaud A *et al* 2006 Micromachined piezoresistive proximal probe with integrated bimorph actuator for aligned single ion implantation *J. Vac. Sci. Technol.* B **24** 3148–51

[57] Schenkel T, Radmilovic V, Stach E A, Park S J and Persaud A 2003 Formation of a few nanometre wide holes in membranes with a dual beam focused ion beam system *J. Vac. Sci. Technol.* B **21**

[58] Alves A D C, Van Donkelaar J, Rubanov S, Reichart P and Jamieson D N 2008 Scanning transmission ion microscopy of nanoscale apertures *J. Korean Phys. Soc.* **53** 3704

[59] Storm A J, Chen J H, Ling X S, Zandbergen H W and Dekker C 2003 Fabrication of solid-state nanopores with single-nanometre precision *Nat. Mater.* **2** 537–40

[60] Danelon C, Santschi C, Brugger J and Vogel H 2006 Fabrication and functionalization of nanochannels by electron-beam-induced silicon oxide deposition *Langmuir* **22** 10711–5

[61] Chen P, Wu M-Y, Salemink H W M and Alkemade P F A 2009 Fast single-step fabrication of nanopores *Nanotechnology* **20** 015302

[62] Herring C 1962 Critique of the Heitler–London method of calculating spin couplings at large distances *Rev. Mod. Phys.* **34** 631–45

[63] Slater J C 1963 *Quantum Theory of Molecules and Solids* vol 1 (New York: McGraw-Hill)

[64] Openov L A 2004 Resonant pulse operations on the buried donor charge qubits in semiconductors *Phys. Rev.* B **74** 233313

[65] Barrett S D and Milburn G J 2003 Measuring the decoherence rate in a semiconductor charge qubit *Phys. Rev.* B **68** 155307

[66] Tsukanov A V 2007 Single-qubit operations in the double-donor structure driven by optical and voltage pulses *Phys. Rev.* B **76** 035328

[67] Koiller B, Hu X and Das Sarma S 2002 Exchange in silicon-based quantum computer architecture *Phys. Rev. Lett.* **88** 027903

[68] Wellard C J, Hollenberg L C L and Das Sarma S 2006 Theory of the microwave spectroscopy of a phosphorus-donor charge qubit in silicon: coherent control in the Si:P quantum-computer architecture *Phys. Rev.* B **74** 075306

[69] Tyryshkin A M, Lyon S A, Schenkel T, Bokor J, Chu J, Jantsch W, Schäffler F, Truitt J L, Coppersmith S N and Eriksson M A 2006 Electron spin coherence in Si *Physica* E **35** 257–63

[70] Lansbergen G P, Rahman R, Wellard C J, Woo I, Caro J, Collaert N, Biesemans S, Klimeck G, Hollenberg L C L and Rogge S 2008 Gate-induced quantum-confinement transition of a single dopant atom in a silicon FinFET *Nat. Phys.* **4** 656–61

[71] Calderón M J, Koiller B and Sarma S D 2007 External field control of donor electron exchange at the Si/SiO_2 interface *Phys. Rev.* B **75** 125311
[72] www.synopsys.com
[73] Koiller B, Hu X and Das Sarma S 2006 Electric-field driven donor-based charge qubits in semiconductors *Phys. Rev.* B **73** 045319
[74] Conrad V I 2007 Designing a solid-state qubit: computational modeling of two level quantum systems in silicon and associated nano-electronics *PhD Thesis* School of Physics, The University of Melbourne
[75] Klimeck G, Oyafuso F, Boykin T B, Bowen R C and Allmen P 2002 Development of a nanoelectronic 3-d (nemo 3-D) simulator for multimillion atom simulations and its application to alloyed quantum dots *Comput. Model. Eng. Sci.* **3** 601–42